NEW RESULTS FROM ALEPH IN e^+e^- ANNIHILATIONS AT $\sqrt{s} = 161$–172 GeV*

P. AZZURRI

Scuola Normale Superiore and INFN Sezione di Pisa
Piazza dei Cavalieri 7, 56010 Pisa, Italy

(Received April 4, 1997)

After the energy upgrade of CERN's LEP electron-positron collider, an integrated luminosity of 22 pb^{-1} has been collected by the ALEPH experiment during the 1996 data taking period, with a centre-of-mass energy of 161 and 172 GeV. With this data, new studies of the standard electroweak theory and of quantum chromodynamics observables are presented and, most notably, precision measurements of m_W are obtained from the first observation of W pair decays. No evidence of Higgs boson production, nor any signal of supersymmetry or other new physics has been found in the data so that limits are derived, in the framework of the SM and of its minimal supersymmetric extension. The anomalous four jet production excess that was reported at lower centre-of-mass energies of 130–136 GeV is partially confirmed with the new data, though the origin of such excess in not yet well understood and necessitates further studies. All the presented ALEPH results are preliminary and subject to modifications.

PACS numbers: 13.10. +q, 13.65. +i, 13.85. Rm, 12.15. -y

1. Introduction

During the 1996 winter shutdown, a major energy upgrade of the LEP electron-positron collider at CERN was accomplished. The storage ring was equipped with additional sets of superconducting RF cavities, bringing the collider fully in the LEP2 phase, with a centre-of-mass energy above the nominal threshold of the $e^+e^- \to W^+W^-$ reaction.

Production of W boson pairs is one of the major goals of the LEP2 program. So far the discovery [1] and studies [2] of W bosons have been achieved with single W productions in $p\bar{p}$ collisions, and in this context the W mass has been measured from large samples of $e\nu_e$ and $\mu\nu_\mu$ decays, to

* Presented at the Cracow Epiphany Conference on W Boson, Cracow, Poland, January 4–6, 1997.

a precision of 125 MeV/c^2 [3]. At LEP2 W's can be detected in all decay modes and the $\sqrt{s}$ annihilation energy can be known precisely. Through the cross-section measurement near the W-pair threshold and by direct kinematic reconstruction of decay products, the W mass determination should improve significantly at LEP2 [4]. A comparison of precision measurements of the W mass, the Z^0 mass and the Fermi constant constitutes a sensitive probe of electroweak radiative corrections, and, together with top quark mass, can give indications on the mass of the Higgs boson, or reveal new physics.

Further test of the standard electroweak theory can be performed at LEP2 energies, through the measurement of fermion pair production cross-sections and of their forward-backward asymmetries, while new QCD studies are possible analysing the properties of hadronic final states.

Besides the above measurements, LEP2 represents also a new era for the search of the yet undiscovered scalar Higgs boson, as predicted by the minimal Standard Model spontaneous SU(2)×U(1) symmetry breaking mechanism. The Higgs boson production is possible at LEP2, via the Higgs-strahlung process $e^+e^- \to HZ^0$, in association with an on-shell Z^0, and such production cross-section is within reach for Higgs masses $m_H < \sqrt{s} - m_Z$.

Finally the increased energy allows for many new searches of physics signals beyond the Standard Model. Most of all new regions and scenarios of possible supersymmetric theories can be explored, hoping for a first evidence of SUSY in nature.

1.1. The 1996 LEP physics runs

Between July and August LEP provided physics collisions at a nominal $\sqrt{s}$ of 161 GeV and, while the first W pair decays were seen at all 4 Interaction Points, ALEPH recorded an integrated luminosity of 11.08 pb^{-1}, when all essential parts of the detector were active. After a technical stop for the installation of more superconducting RF cavities, the 1996 run resumed in October and November, when ALEPH collected 0.04 pb^{-1} at $\sqrt{s}$ =164 GeV, 1.11 pb^{-1} at $\sqrt{s}$ =170 GeV and 9.54 pb^{-1} at $\sqrt{s}$ =172 GeV.

The great precision beam energy determination obtained at LEP1 using resonant depolarisation of the circulating beam [5] was not possible at LEP2 energies, since it has so far proved impossible to obtain useful levels of polarisation at beam energies above 50 GeV. Therefore LEP2 beam energies have been determined via an extrapolation from the depolarisation-measured energies close to the Z^0 peak, at 45–50 GeV per beam, to the 80.5–86 GeV beam energies, by the use of the NMR probes which measure continually the field in 16 dipoles of the tunnel [6]. Table I summarises the integrated luminosities and averaged energies recorded by ALEPH during the different 1996

LEP2 data taking periods. The energy uncertainties are dominated by the uncertainty in the extrapolation of the NMR fields from the depolarisation calibrations.

For most of the following physics studies the data taken at 164 GeV is ignored, while the data taken at 170 and 172 GeV has been merged into a total of 10.650 ± 0.076 pb^{-1} of data with a luminosity-weighted $\sqrt{s} = 172.086 \pm 0.060$ GeV.

TABLE I

Integrated luminosities and average energies recorded by ALEPH for each different nominal energy run period delivered by LEP in 1996.

Nominal $\sqrt{s}$ (GeV)	L (pb^{-1})	Measured $\sqrt{s}$ (GeV)
161	11.076 ± 0.080	161.314 ± 0.054
164	0.041 ± 0.003	164.531 ± 0.060
170	1.114 ± 0.016	170.283 ± 0.060
172	9.536 ± 0.069	172.297 ± 0.060

2. The ALEPH detector

A detailed description of the ALEPH detector can be found elsewhere [7], as well as an account of its performances and a description of the standard analysis algorithms [8].

Charged particles are detected in the central part of the detector, consisting of three subdetectors. The silicon vertex detector (VDET) [9] is the closest to the beam crossing point with two concentric layers at radii 6.3 and 11.0 cm. For tracks passing through VDET, the resolution on the impact parameter with respect to the primary interaction point, can be parameterised as $\Delta\delta = (34 + 70/p(\mathrm{GeV}/c))(1 + 1.6\cos^4\theta))$ μm. VDET is surrounded by a cylindrical multiwire drift chamber (ITC) [10] and by a large time projection chamber (TPC) [11]. The TPC is the principal tracking chamber of the ALEPH detector and for each track, in addition to space coordinates, it can determine up to 338 samples of ionisation energy loss dE/dx, that serve to separate particle species, according to their momentum. The three tracking devices are contained within a 1.5 T axial magnetic field and measure up to 31 coordinates along the particle trajectories, yielding a momentum resolution $\Delta p/p = 0.6 \times 10^{-3} p_T(\mathrm{GeV}/c) \oplus 5 \times 10^{-3}$. Hereafter, reconstructed charged tracks originating from within a cylinder of 2 cm radius and 20 cm length, centred on the nominal interaction point and parallel to the beam axis, are called *good* tracks.

The tracking chambers are surrounded by a lead/proportional-chamber electromagnetic calorimeter (ECAL), with fine read-out segmentation and

22 radiation lengths of thickness at normal incidence. ECAL provides an electromagnetic energy measurement resolution $\Delta E/E = 0.18/\sqrt{E(\mathrm{GeV})} \oplus 0.009$. Electrons and photons are identified in ECAL by their characteristic longitudinal and transverse shower developments. The hadron calorimeter (HCAL) consists of the magnet return yoke instrumented with 23 layers of streamer tubes, the total thickness corresponds to 7 interaction lengths at normal incidence and the energy resolution obtained for hadronic showers is $\Delta E/E = 0.85/\sqrt{E(\mathrm{GeV})}$. Muons are identified by their penetration pattern in HCAL and in the two outer layers of muon chambers.

The total visible energy is measured with an energy-flow reconstruction algorithm [8] which combines all of the above measurements, supplemented at low polar angles by the energy detected in the luminosity calorimeters. Making use of the detector identification capabilities of photons, electrons and muons, the algorithm also provides a list of charged and neutral reconstructed objects (*energy-flow particles*), characterised by their energies and momenta from which hadronic jets are reconstructed with clustering algorithms. The resulting jet energy resolution is $\Delta E(\mathrm{GeV}) = (0.6\sqrt{E(\mathrm{GeV})} + 0.6)(1 + \cos^2\theta)$, where θ is the polar angle of the jet axis. Jets originating from b quarks are identified from lifetime tagging algorithms, from high transverse momentum leptons from semileptonic b-decays and with jet shape variables, combined together [12].

Luminosity is measured with small angle Bhabha events, using lead-proportional wire sampling calorimeters, covering polar angles from 45 to 169 mrad on both sides of the interaction point [13]. The accepted Bhabha cross-section is 5.9 nb [14], background contaminations are less than 0.1% while systematic uncertainties on the integrated luminosity measurements account for 0.6%.

3. Fermion pairs production

Hadron and lepton-pair productions have been studied by ALEPH around the Z^0 resonance at $\sqrt{s} \simeq 91$ GeV (LEP1) [15] and at $\sqrt{s} =$ 130–136 GeV (LEP1.5) [16]. At centre-of-mass energies above the Z^0, for a large number of events, initial state photon radiation (ISR) lowers the invariant mass $\sqrt{s'}$ of the final state fermions to values close to m_Z. These are called radiative Z-returns as the event in Fig. 1. Cross-sections and asymmetries for $\sqrt{s'}$ values closer to the nominal $\sqrt{s}$ are instead more sensitive to the relevant high-energy electroweak effects. Therefore two different fermion pair production conditions are defined: the exclusive, non-radiative interaction with $\sqrt{s'/s} > 0.9$ and the inclusive interaction with $\sqrt{s'/s} > 0.1$.

The event selection techniques are similar to the ones used for previous studies and are described in detail in Ref. [16]. The common lepton-pair

selection includes requirements on the multiplicity, energy and topology of the event *good* charged tracks. Further cuts on transverse momentum and visible mass are applied against the $\gamma\gamma \to \ell^+\ell^-$ background.

For all lepton pairs the scattering angle θ^* in the $\ell^+\ell^-$ rest frame is estimated as $\cos\theta^* = \cos\frac{1}{2}(\theta_- + \pi - \theta_+) / \cos\frac{1}{2}(\theta_- - \pi + \theta_+)$ where θ_+ and θ_- are the measured polar angles of the final state leptons. An approximate value of $\sqrt{s'}$ is also obtained as:

$$s'_m = s\frac{\sin\theta_+ + \sin\theta_- - |\sin(\theta_+ + \theta_-)|}{\sin\theta_+ + \sin\theta_- + |\sin(\theta_+ + \theta_-)|}. \tag{1}$$

Only events with $\sqrt{s'_m/s} > 0.9$ are accepted for the non-radiative selection.

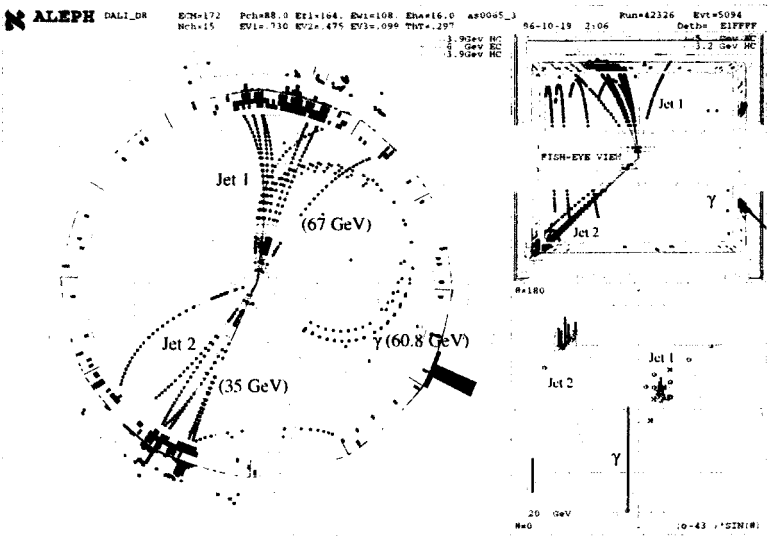

Fig. 1. An hadronic radiative return to the Z^0 peak at $\sqrt{s} = 172$ GeV, $e^+e^- \to q\bar{q}\gamma$ where the photon is visible in the detector.

Hadronic events are selected by requiring at least 5 *good* charged tracks and a visible mass above 50 GeV. The measurement of s'_m is then performed after removing ISR photons in the detector, again $\sqrt{s'_m/s} > 0.9$ is required for the non-radiative selection. The main backgrounds to the hadronic selections are WW and ZZ^* events. All the selection backgrounds and signal efficiencies have been evaluated with fully reconstructed simulated events generated with **PYTHIA** [17] for $q\bar{q}$, **KORALZ** [19] for $\tau^+\tau^-$ and $\mu^+\mu^-$, and **UNIBAB** [20] for e^+e^-.

TABLE II

Summary of ALEPH preliminary $f\bar{f}$ cross sections and forward-backward asymmetries at $\sqrt{s} = 161$ and 172 GeV. The first error comes from statistical fluctuations and the second is due to systematic uncertainties. The e^+e^- cross sections are given for (1) $-0.9 < \cos\theta^* < 0.9$ and (2) $-0.9 < \cos\theta^* < 0.7$.

	$\sqrt{s} = 161$ GeV		
	$\sigma(\sqrt{s'/s} > 0.1)$ (pb)	$\sigma(\sqrt{s'/s} > 0.9)$ (pb)	$A_{FB}(\sqrt{s'/s} > 0.9)$
$q\bar{q}$	$148.56 \pm 3.87 \pm 1.93$	$32.06 \pm 1.68 \pm 1.46$	
$\tau^+\tau^-$	$10.78 \pm 1.34 \pm 0.42$	$4.03 \pm 0.76 \pm 0.16$	$0.525 \pm 0.19 \pm 0.021$
$\mu^+\mu^-$	$12.88 \pm 1.21 \pm 0.13$	$5.96 \pm 0.79 \pm 0.07$	$0.740 \pm 0.096 \pm 0.019$
e^+e^- (1)		$129.16 \pm 3.68 \pm 1.05$	
e^+e^- (2)		$28.92 \pm 1.68 \pm 0.34$	
	$\sqrt{s} = 172$ GeV		
	$\sigma(\sqrt{s'/s} > 0.1)$ (pb)	$\sigma(\sqrt{s'/s} > 0.9)$ (pb)	$A_{FB}(\sqrt{s'/s} > 0.9)$
$q\bar{q}$	$124.93 \pm 3.70 \pm 2.11$	$30.99 \pm 1.66 \pm 1.45$	
$\tau^+\tau^-$	$10.94 \pm 1.32 \pm 0.3$	$4.23 \pm 0.78 \pm 0.13$	$0.478 \pm 0.214 \pm 0.022$
$\mu^+\mu^-$	$9.96 \pm 1.09 \pm 0.13$	$4.50 \pm 0.69 \pm 0.05$	$0.719 \pm 0.118 \pm 0.021$
e^+e^- (1)		$109.92 \pm 3.43 \pm 0.63$	
e^+e^- (2)		$23.97 \pm 1.51 \pm 0.10$	

A summary of inclusive and non-radiative ALEPH two-fermion cross-sections and asymmetries at $\sqrt{s} = 160 - 172$ GeV are shown in Table II. The $\sqrt{s}$-dependence of ALEPH results are compared with the SM in Fig. 2.

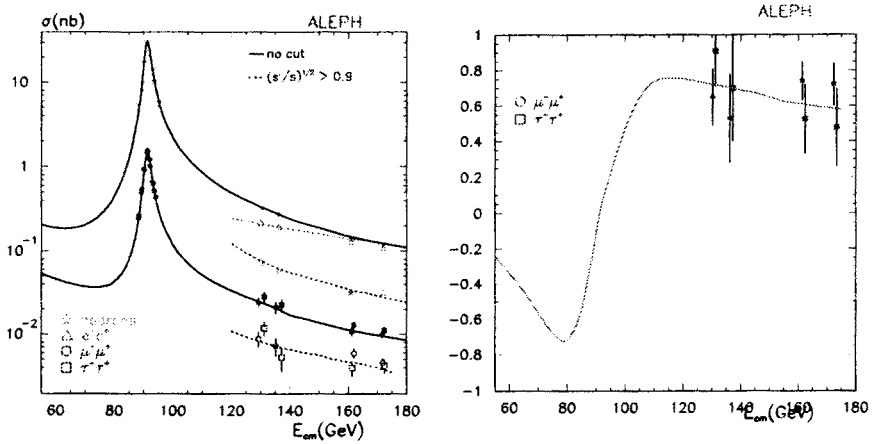

Fig. 2. ALEPH preliminary $f\bar{f}$ cross sections and forward-backward asymmetries, and their comparison with the SM.

From the S-matrix formalism for the hadronic cross section, the γ–Z interference contribution $j^h_{\rm tot}$ can be fitted with all ALEPH measured hadronic cross sections from $\sqrt{s} = M_Z$ to 172 GeV, leading to $j^h_{\rm tot} = -0.095 \pm 0.319$, to be compared with the SM prediction $j^h_{\rm tot} = 0.22$.

4. Quantum Chromodynamics studies in $q\bar{q}$ events

The non-radiative hadronic $q\bar{q}$ final states collected by ALEPH at $\sqrt{s}$ =161–172 GeV have been analysed to measure quantities for which the $\sqrt{s}$-dependence can be predicted by QCD, compared with the same kind of measurements done both at $\sqrt{s} = M_Z$ [21] and at $\sqrt{s}$ =130–136 GeV [22]. The $\sqrt{s}$-dependence of inclusive hadronic particle distributions can be predicted once they have been determined at a single energy, while infrared finite quantities, such as jet rates and event-shape distributions, can be computed perturbatively as a function of the running constant $\alpha_S(s)$. In these cases, by going to higher energies, the $\sqrt{s}$-dependence can be checked in a regime where non-perturbative effects are expected to decrease.

All measured distributions have been corrected for detector effects and efficiencies, by means of bin-by-bin correction factors computed using the **PYTHIA** [17] and **JETSET** [18] Monte Carlo generators with full detector simulation. Together with **PYTHIA**, also the **HERWIG** [23] and **ARIADNE** [24] models have been used for comparison, all tuned with the $\sqrt{s} = M_Z$ data, and differences have been taken into account when estimating the systematic errors.

The selection of $q\bar{q}$ events for QCD studies requires at least 7 *good* charged tracks with a total energy greater than $0.1\sqrt{s}$, and the sphericity axis polar angle $|\cos\theta_{\rm sph}| < 0.9$. Subsequently hard cuts are applied to eliminate hadronic radiative Z^0-returns and reduce the WW only contamination to a total background of 7.5% for the $\sqrt{s} = 172$ GeV selection.

TABLE III

Inclusive charged multiplicity and global event thrust means measured in ALEPH $q\bar{q}$ at $\sqrt{s} = 161 - 172$ GeV. Errors are statistical and systematic.

	$\sqrt{s} = 161$ GeV	$\sqrt{s} = 172$ GeV
$\langle N_{\rm ch} \rangle$	$26.53 \pm 0.41 \pm 0.38$	$26.33 \pm 0.44 \pm 0.41$
$\langle 1 - T \rangle$	$0.0610 \pm 0.0039 \pm 0.0029$	$0.0532 \pm 0.0043 \pm 0.0039$

Inclusive charged particle distributions have been measured for the variables $x_p = p/p_{\rm beam}$ (scaled momentum), y (rapidity with respect to the thrust axis), $p_\perp^{\rm in}$ and $p_\perp^{\rm out}$ (transverse momentum in and out of the event plane) [21]. All measured distributions are in agreement with QCD models

and, from the integral of the rapidity distribution, the mean multiplicity of charged particles has been determined as in Table III. The energy dependence of $\langle N_{\rm ch} \rangle$ is shown in Fig. 3, and confirms that multiple gluon emission, not well simulated in $O(\alpha_S^2)$ models, is necessary to describe such dependence.

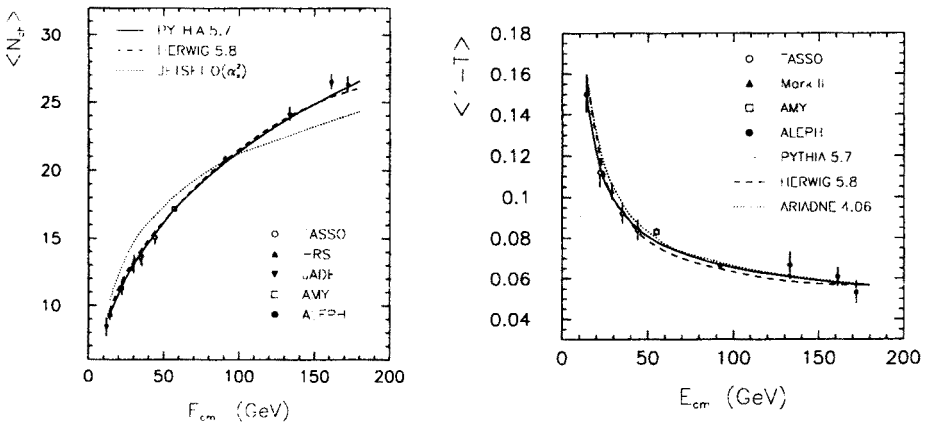

Fig. 3. ALEPH preliminary Mean multiplicity of inclusive charged particles $\langle N_{\rm ch} \rangle$ and of the global event-shape thrust $\langle 1 - T \rangle$, as a function of $\sqrt{s}$, compared to the prediction of QCD Monte Carlo models.

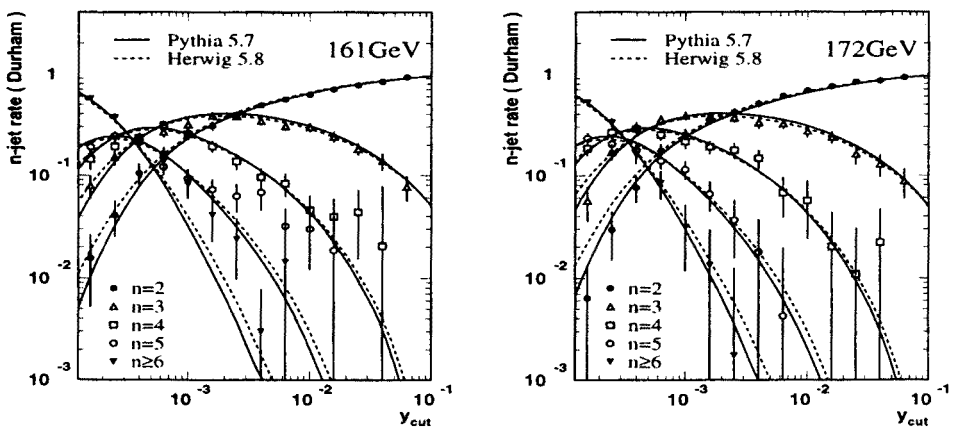

Fig. 4. ALEPH preliminary $q\bar{q}$ Durham n-jets rates for n = 2,3,... with different $y_{\rm cut}$ values, and the predictions of Monte Carlo models, at $\sqrt{s} = 161 - 172$ GeV.

Global hadronic event structure variables have also been considered, as the event thrust T, the differential two-jet rate y_3 and the n jet rates. The thrust is defined with all the *energy-flow* particles in the event as

$T = \max\left(\sum_j |p_{\|j}| / \sum_j |p_j|\right)$, its distributions were found in reasonable agreement with the QCD models and the mean values are in Table III. The $\sqrt{s}$-dependence of $\langle 1 - T \rangle$ is also plotted in Fig. 3.

Jet rates and y_3 are built by means of the Durham clustering algorithm [26]. The measured and predicted jet-rates, at different $y_{\rm cut}$ clustering values, are shown in Fig. 4. Some excess can be observed for the production of $n \geq 5$ jets at 161 GeV, such excess disappears in the 172 GeV data.

The determination of the strong coupling constant α_S has been done from a fit to the $L = -\ln y_3$ distribution in the fit range $1.2 < L < 7.6$, as in previous studies [22]. The results are:

$$\alpha_S(161\ \text{GeV}) = 0.1085 \pm 0.0045(\text{stat}) \pm 0.0020(\text{syst}) \pm 0.0004(\text{hadr}) \pm 0.0047(\text{theo})$$

$$\alpha_S(172\ \text{GeV}) = 0.1082 \pm 0.0050(\text{stat}) \pm 0.0024(\text{syst}) \pm 0.0004(\text{hadr}) \pm 0.0045(\text{theo})$$

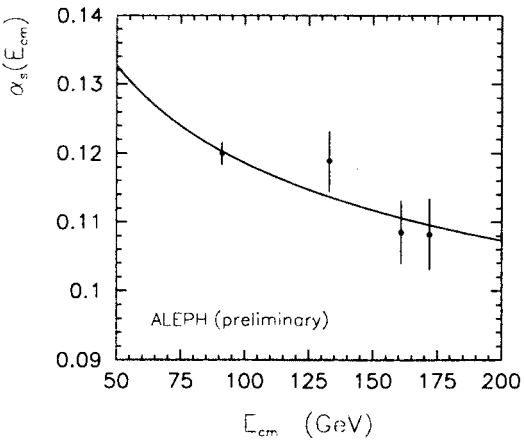

Fig. 5. Running of α_S with ALEPH determinations at different energies. The theory error is not included as it is almost fully correlated between different $\sqrt{s}$.

5. W pairs production

The SM production of W pairs in e^+e^- collisions is described, at lowest-order, by three diagrams with two charged current resonating W bosons, or CC03 diagrams, showed in Fig. 6 together with the $\sqrt{s}$-dependence of the total WW cross-section, with all relevant corrections.

Near the kinematic threshold such WW cross section retains a rapid increase and a remarkable dependence from m_W, so that measuring the WW cross-section σ_{WW} yields indirectly a measurement of m_W. For a fixed

luminosity, selection efficiency and backgrounds, the maximum statistical sensitivity to m_W is obtained for a minimum $\sqrt{\sigma_{WW}}|dm_W/d\sigma_{WW}|$ factor, at the optimal threshold energy of $\sqrt{s} \simeq 2m_W + 0.5$ GeV $\simeq 161$ GeV, that was chosen for this reason for the first LEP2 running period.

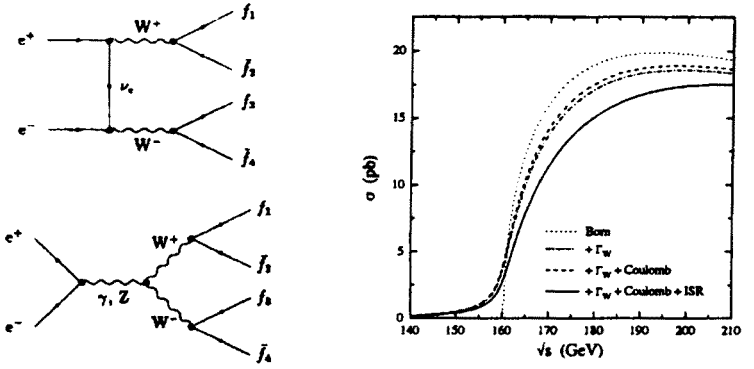

Fig. 6. W pair production in e^+e^- collisions. SM CC03 production diagrams and $\sqrt{s}$-dependence near the threshold.

Each CC03 diagram leads to an experimentally accessible four-fermion final state, but many other SM processes can lead to the same four-fermion final states as W pair decays, interfering with the CC03 ones. The contribution of these non-CC03 diagrams can be very large for final states containing electrons or $f\bar{f}$ pairs, however their effect reduces to a few percent when requiring, as for event selections, that all four-fermions are separated and within the detector acceptance. In this situation the effect of the non-CC03 diagrams is corrected for by comparing Monte Carlo simulations including a) only CC03 processes, and b) the full four-fermion production.

The extraction of the pure CC03 cross-section proceeds defining, from Monte Carlo, a *four fermion to CC03* correction, for all WW decay modes, as $\Delta\sigma_{\overline{\text{CC03}}} = \left[\varepsilon_{4f}\sigma^{\text{MC}}_{4f} - \varepsilon_{\text{CC03}}\sigma^{\text{MC}}_{\text{CC03}}\right]$, where ε_{4f} and $\varepsilon_{\text{CC03}}$ are the selection efficiencies obtained with the full four-fermion and the CC03 Monte Carlo samples. The measured CC03 cross-section is then obtained as

$$\sigma_{\text{CC03}} = \frac{N_{\text{obs}}/\mathcal{L} - \sigma_{\text{back}} - \Delta\sigma_{\overline{\text{CC03}}}}{\varepsilon_{\text{CC03}}}, \tag{2}$$

where N_{obs} is the number of observed events, $\mathcal{L}$ the collected luminosity and σ_{back} the amount of other physics backgrounds. The full ALEPH signal and four-fermion simulation have been done using different m_W values, with the KORALW [27] and EXCALIBUR [28] event generators.

The selection of W pair events are essentially identical at 161 and 172 GeV, as only some cuts and criteria have been rescaled with the centre-of-mass energy, and minor different re-optimisations have been done for the two different energies. Up to $\sqrt{s} = 172$ GEV, W's are produced with low velocities so that the resulting four-fermion momenta are around 40 GeV each and tend to be back-to-back in pairs. This peculiar kinematic configuration is fundamental for the selection criteria of all decay modes.

5.1. Selection of $q\bar{q}q\bar{q}$ decays

Fully hadronic WW decays are characterised by no missing energy or momentum and a large multiplicity of charged and *energy-flow* objects, as in Fig. 7. The largely dominant background comes from non-radiative hadronic $q\bar{q}$ events with hard QCD gluon emission and multijet spherical topologies.

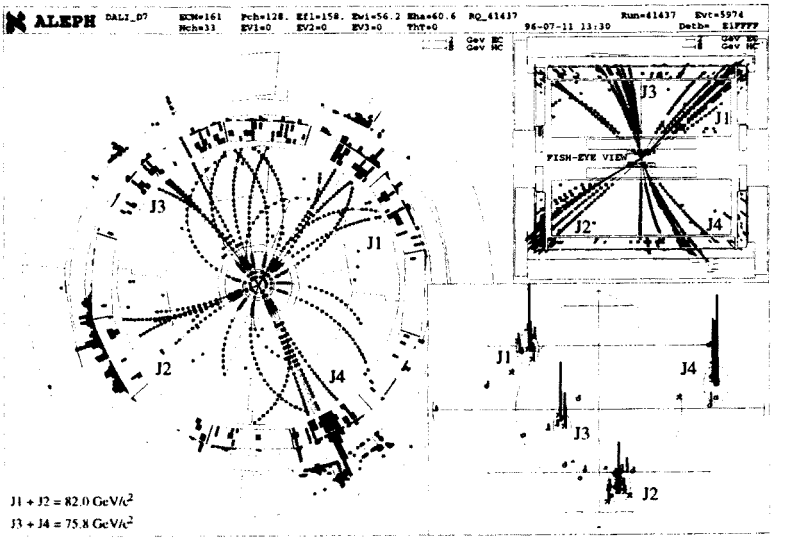

Fig. 7. The first W pair seen in ALEPH at $\sqrt{s} = 161$ GeV as a four jet decay.

After a simple preselection of hadronic non-radiative events with a topology of four *hard* jets, each with high energies and multiplicities, several variables are built to discriminate signal events from QCD backgrounds. These variables are mostly based on the kinematics of the four jets, as inter-jet angles, y_{34} and di-jet masses, and also global topological variables, as the event sphericity. Four different multivariable methods have been employed to combine the information of each distribution and discriminate optimally signal from background, they are:

1. A linear discriminant analysis, where a single variable is built as a linear combination of 14 input variables, optimising its separation power of signal and background.
2. A feed-forward neural net, trained with back-propagation with 9 input variables, and an output between 0 (background) and 1 (signal).
3. A rarity method, where the rarity of an event is defined in a input 6-dimensional space as the (integrated) fraction of signal events with worse (or more background-like) coordinates than the measured ones.
4. A weighting method, where the 5-dimensional input space is binned, and each event weight is defined as the (local) fraction of signal in that bin.

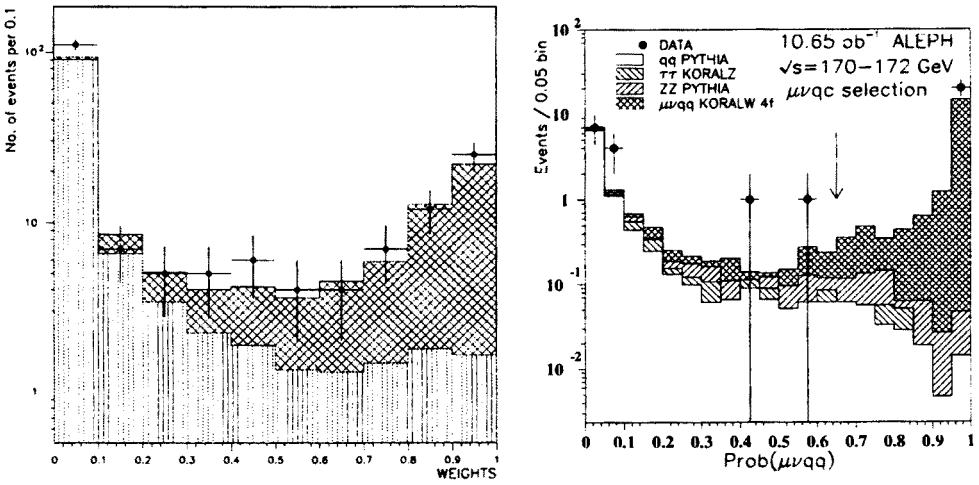

Fig. 8. ALEPH preliminary (a) Weights distribution for preselected $q\bar{q}q\bar{q}$ events at $\sqrt{s} = 172$ GeV. The hatched area at higher weights is the fitted WW contribution, the shaded area the QCD background. (b) Probability output of preselected $\mu\nu q\bar{q}$ events. The arrow shows the cut applied to separate signal from backgrounds.

For each method the WW hadronic cross-section is obtained by fitting the data output distribution shape as the one in Fig. 8. The four obtained cross-sections are finally combined together taking into account their large correlations, as measured from Monte Carlo. Such combined results are summarised in Table IV.

TABLE IV

ALEPH preliminary CC03-corrected cross sections for W pair decay modes. The first error is statistical, the second comes from systematic uncertainties.

decay mode	$\sqrt{s} = 161$ GeV	$\sqrt{s} = 172$ GeV
$q\bar{q}q\bar{q}$	$1.80 \pm 0.50 \pm 0.19$ pb	$5.76 \pm 0.88 \pm 0.22$ pb
$e\nu q\bar{q}$		$1.42^{+0.46}_{-0.32} \pm 0.06$ pb
$\mu\nu q\bar{q}$		$1.97^{+0.50}_{-0.43} \pm 0.05$ pb
$\tau\nu q\bar{q}$		$1.28^{+0.80}_{-0.72} \pm 0.07$ pb
$\ell\nu q\bar{q}$	$1.85^{+0.51}_{-0.43} \pm 0.06$ pb	$4.73^{+0.80}_{-0.72} \pm 0.16$ pb
$\ell\nu\ell\nu$	$0.68^{+0.34}_{-0.26} \pm 0.03$ pb	$1.22 \pm 0.40 \pm 0.06$ pb
Total (SM)	$4.23^{+0.75}_{-0.71}0.19\pm$ pb	$11.68^{+1.27}_{-1.23} \pm 0.25$ pb

5.2. Selection of $\ell\nu q\bar{q}$ decays

In semileptonic WW events, the primary neutrino carries about 40 GeV of energy and momentum, and in one third of the cases, when the lepton is a tau, additional energy is lost in neutrinos from its decay. The key feature of these events is that the lepton, or the thin τ decay jet, points in a roughly opposite direction to the missing momentum and is well separated from the two hadronic jets. For all lepton flavours, preselection criteria are applied to select hadronic events with missing momentum $\not{p}$ out of the beam axis direction.

In $e\nu q\bar{q}$ and $\mu\nu q\bar{q}$ decays the lepton is identified as the charged track with the highest momentum antiparallel to $\not{p}$, then electron and muon identification criteria are applied to reduce background events. After this the probability for an event to come from the signal process is evaluated multidimensionally using 1) the missing transverse momentum, 2) the lepton energy and 3) the lepton isolation from the remaining hadronic system. Finally events are selected using a cut on the probability output that minimises the Monte Carlo expected statistical error on the cross-section.

For $\tau\nu q\bar{q}$ events two selections were designed. In a topological selection jets are built with the JADE algorithm [25] ($y_{\rm cut} = 10^{-3}$), and the single track jet most opposite to $\not{p}$ is chosen as the τ-jet; further requirements are applied on the τ-jet energy and isolation, and on the remaining hadronic system. A second, global, selection relies on the fact that $\tau\nu q\bar{q}$ events are acollinear and acoplanar, and that the missing momentum is isolated in space.

All semileptonic analyses are combined inclusively with overall CC03-efficiencies of 77.2% at 161 GeV and 81.4% at 172 GeV. Separate cross-

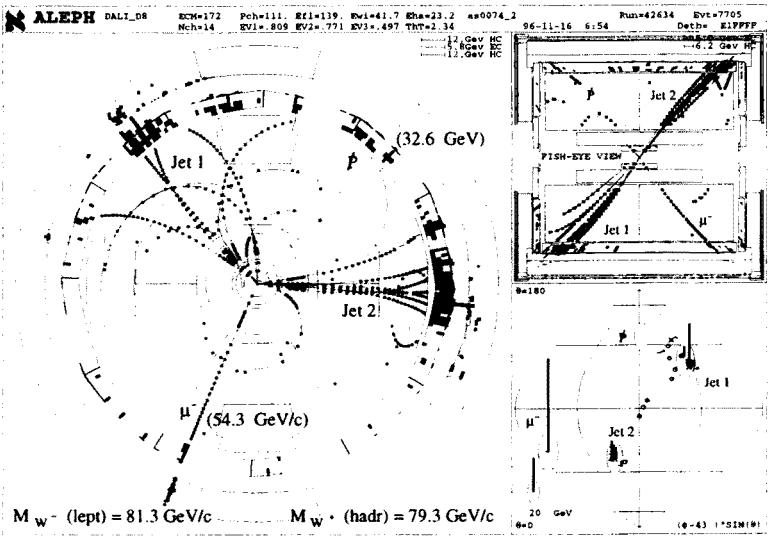

Fig. 9. A W pair seen in ALEPH at $\sqrt{s} = 172$ GeV as a $\mu\nu q\bar{q}$ decay.

sections for each lepton flavour have been determined at 172 GeV by means of a Poisson probability maximum likelihood fit to each analysis selected events and overlaps. All measured partial and total semileptonic cross-sections are listed in Table IV.

5.3. Selection of $\ell^+\nu\ell^-\bar{\nu}$ decays

This channel is characterised by two acoplanar energetic leptons and a large missing energy carried away by the corresponding neutrinos. In 5/9 of the events at least one lepton is a tau, giving rise to softer final states and additional missing energy. A low multiplicity of *good* tracks is required in the selection as well as a large missing transverse momentum and acoplanarity $\Delta\phi$ in the plane transverse to the beam axis. Further cuts are applied to reduce radiative dilepton and $\gamma\gamma \to \ell^+\ell^-$ backgrounds, especially against tau pairs, leading to efficiencies of 70.4-72.5% at 161–172 GeV.

5.4. Combination of cross-sections and m_W extraction

The results from all WW decay channels have been combined using a maximum likelihood fit with Poisson statistics. The total WW cross-sections have been extracted forcing the Standard Model W branching ratios in the fit. All the partial and total CC03-corrected cross-sections are listed in Table IV, where the central values of partial results don't necessarily sum up to the total ones, as they are obtained with such likelihood fit procedures.

Assuming only lepton universality, the W hadronic branching ratio has been fitted together with the total 172 GeV cross-sections, obtaining

$$Br(W \to q\bar{q}') = 69.4^{+3.5}_{-3.7}(\text{stat}) \pm 0.8(\text{syst})\%$$

that represents a first direct precision measurement of W branching ratios obtainable at LEP2.

The W mass was obtained from the total WW cross-sections within the Standard Model framework, using the **GENTLE** program [29]. Using only the 161 GeV cross-section the result is:

$$m_W = 80.14 \pm 0.34(\text{stat}) \pm 0.09(\text{syst}) \pm 0.03(\text{LEP}) \text{ GeV}/c^2,$$

while fitting both WW cross-sections at 161 and 172 GeV gives:

$$m_W = 80.20 \pm 0.33(\text{stat}) \pm 0.09(\text{syst}) \pm 0.03(\text{LEP}) \text{ GeV}/c^2,$$

where the last error comes from the uncertainty on the LEP beam energy.

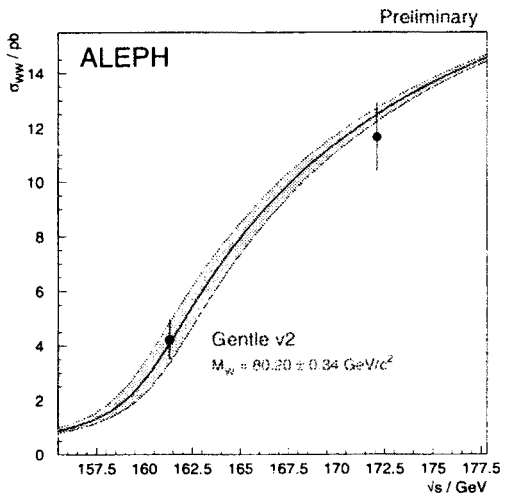

Fig. 10. Total WW cross sections measured by ALEPH at $\sqrt{s}$ =161 and 172 GeV. The shaded area shows the corresponding SM fitted m_W values, with errors.

5.5. Kinematic reconstruction of the W mass

With the $q\bar{q}q\bar{q}$ and $\ell\nu q\bar{q}$ decays of W pairs, collected mainly at $\sqrt{s}$ = 172 GeV, a direct measurement of the W mass can be achieved, independently from the cross-section indirect yields, by the kinematic reconstruction of each W decay products [4].

Selected $q\bar{q}q\bar{q}$ W-pair decays are reconstructed into 4 jets with the Durham P-scheme [26] algorithm; the jet momenta are then refitted constraining total energy and momentum conservation (4C fit), using a covariance matrix for the jet errors, with a dependence from the jet energy and angles which reflects the detector response to the hadronisation decay products. The refitted jets are then paired into the most probable configuration for a W-pair decay by means of an iterative procedure, and each dijet mass is rescaled, to obtain a more precise mass estimate, as $m_W{}^r = m_{jj} \cdot (E_{\rm beam}/E_{jj})$. Finally the two rescaled masses obtained for each $q\bar{q}q\bar{q}$ decay are combined together with their expected correlation, obtaining a single m_W measurement.

In selected $\ell\nu q\bar{q}$ decays, the neutrino momentum is defined to be the total missing momentum and the two hadronic jets are refitted, according to their expected errors, with the remaining kinematic constraint of total energy conservation, and the additional one of equality for leptonic and hadronic W masses (2C). In this way a single m_W value is obtained directly for each $\ell\nu q\bar{q}$ decay.

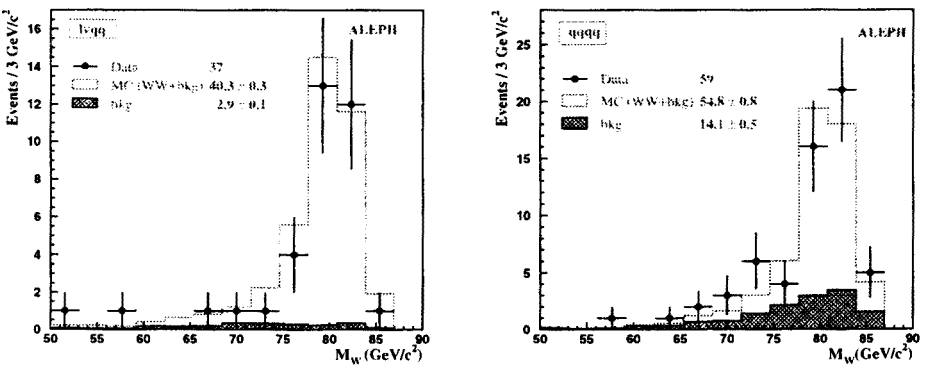

Fig. 11. ALEPH preliminary Reconstructed m_W peaks at $\sqrt{s} = 172$ GeV in the $\ell\nu q\bar{q}$ and $q\bar{q}q\bar{q}$ decay channels.

The distribution of refitted and rescaled masses is shown in Fig. 11. The central m_W value is extracted by means of an unbinned maximum likelihood fit of these distributions to a relativistic Breit–Wigner function. To correct for effects as ISR, jet reconstruction and kinematic refitting, calibration curves have been built from Monte Carlo samples with different input m_W values, to control the biases and non-linearities of the final mass estimator. Finally the central m_W reconstructed values are listed in Table V. Combining the direct W reconstruction results with the information from WW cross-

section measurements, the overall ALEPH m_W average from the 161–172 GeV data is :

$$m_W = 80.39 \pm 0.23(\text{stat}) \pm 0.08(\text{syst}) \quad \text{GeV}/c^2.$$

TABLE V

Preliminary m_W values from direct mass reconstruction of selected WW decays at $\sqrt{s} = 172$ GeV.

WW decay	$m_W\,(\text{GeV}/c^2)$
$q\bar{q}q\bar{q}$	$80.64 \pm 0.45(\text{stat}) \pm 0.18(\text{syst})$
$\ell\nu q\bar{q}$	$80.51 \pm 0.51(\text{stat}) \pm 0.06(\text{syst})$
All	$80.58 \pm 0.34(\text{stat}) \pm 0.10(\text{syst})$

5.6. Anomalous gauge boson couplings

Direct measurements of the trilinear self-couplings of the W, Z and photon (TGC) is possible at LEP2, principally via the pair production of electroweak bosons, and should either corroborate the specific non-abelian Standard Model predicted structure, or reveal New Physics [30]. The trilinear vertex of interest for W-pair production is the WWV one ($V \equiv$Z or γ), and has been quantitatively parametrised with a general structure by means of the well-known coupling coefficients g_i^V, λ_V, κ_V, $\tilde{\lambda}_V$ and $\tilde{\kappa}_V$, or by the C and P conserving parameters x_V, y_V and δ_Z.

Nevertheless, for LEP2, it is more desirable to render the TGC parameterisations gauge invariant, and with a small dependence from the bounds of the lower energy data. The chosen parameters represent therefore C and P conserving couplings in LEP1 *blind directions*, they are written in terms of unmixed gauge bosons (B,W) and Higgs fields (ϕ), and, with respect to the original conventions, are:

$$\alpha_W = y_\gamma \qquad \alpha_{B\phi} = x_\gamma - \delta_Z \sin\theta_W \cos\theta_W \qquad \alpha_{W\phi} = \delta_Z \sin\theta_W \cos\theta_W .$$

Selected $\ell\nu q\bar{q}$ W-pair decays have been used to perform single maximum likelihood fits to each of these 3 parameters, fitting both the total cross-sections, trough the Poisson distribution of selected events, as well as the phase-space configuration of the outgoing fermions, all as a function of the couplings. The likelihood profiles are finally used to set independent 95% CL limits on each anomalous coupling, resulting in

$$-0.94 < \alpha_W < 0.69 \qquad -1.76 < \alpha_{B\phi} < 2.35 \qquad -0.68 < \alpha_{W\phi} < 0.42$$

and showing good agreement with the SM null expectations.

6. Standard Model and MSSM Higgs searches

Within the LEP2 energy reach, the dominant production mechanism for the minimal Standard Model Higgs boson is the Higgs-strahlung process $e^+e^- \to HZ$, where it is produced in association with an on-shell Z^0. Such SM production cross-section is predicted to be about 1 pb for $m_H \sim 65$ GeV/c^2 and fall at the kinematic limit $m_H = \sqrt{s} - m_Z$. In minimal SM extensions with two Higgs doublets, five physical states are observable as neutral CP-even h^0 and H^0, CP-odd A^0 and charged $H^\pm$, and at least two independent parameters are required: $\tan\beta$, ratio of the doublet vacuum expectations, and α, mixing angle in the CP-even sector. In the most popular Minimal Supersymmetric extension of the Standard Model (MSSM), the lighter bosons, h and A, can be produced at LEP2 still via $e^+e^- \to hZ$ Higg-strahlung, suppressed by a factor $\sin^2(\beta - \alpha)$ with respect to the SM, and by the $e^+e^- \to hA$ pair-production, proportional to $\cos^2(\beta - \alpha)$.

Both the HZ and hA productions have been searched for in the 161 and 172 GeV ALEPH data, accounting for all possible Z decay modes (e^+e^-, $\mu^+\mu^-$, $\tau^+\tau^-$, $\nu\bar{\nu}$ and $q\bar{q}$), and for the expected decay modes of each neutral Higgs to $\tau^+\tau^-$ (8%) and $b\bar{b}$ (92%). The **HZHA** generator [31] has been used to simulate all kinds of signal events.

For Higgs-strahlung decays, five different topologies have been searched for as $\tau^+\tau^-\ell^+\ell^-$, $q\bar{q}\ell^+\ell^-$, $b\bar{b}\nu\bar{\nu}$, $q\bar{q}\tau^+\tau^-$ and $q\bar{q}b\bar{b}$, where the last four-jet final state accounts for about 70% of all HZ decays. Further MSSM hA pair-productions have been searched for as $\tau^+\tau^-b\bar{b}$ (14%) and $b\bar{b}b\bar{b}$ (84%) decays.

Final states with b-jets from Higgs-decays have been tagged with a neural net that combines information from lifetime variables, high p_T leptons and jet-shape properties, while associated Z^0 productions can be identified through the selected dijet and lepton pairs invariant masses, or with the total missing mass, in the hypothesis of a $\nu\bar{\nu}$ decay. Dedicated cuts are used to remove radiative fermion pairs and low-angle $\gamma\gamma$ collisions, as well as $We\nu$ and Zee processes. More severe SM four-fermion backgrounds come from WW and $Z\gamma^*$ decays, and are removed by means of an explicit kinematic reconstruction of their decay products. The dominant systematic uncertainty on the selections comes from the knowledge of the b-tagging, and results in an error of ~2%.

From the data samples collected at 161 and 172 GeV no candidate of Higgs productions have been found by any of the selection procedures. therefore all the analyses have been combined in the optimal way, such that the best expected Higgs mass exclusion value would be obtained a-priori, with 95% Confidence Level.

In the SM the confidence level curves, as a function of m_{H}, are shown in Fig. 12. Combining the ALEPH data from LEP1 and LEP2 results in the 95% CL lower limit $m_H < 70.7$ GeV/c^2.

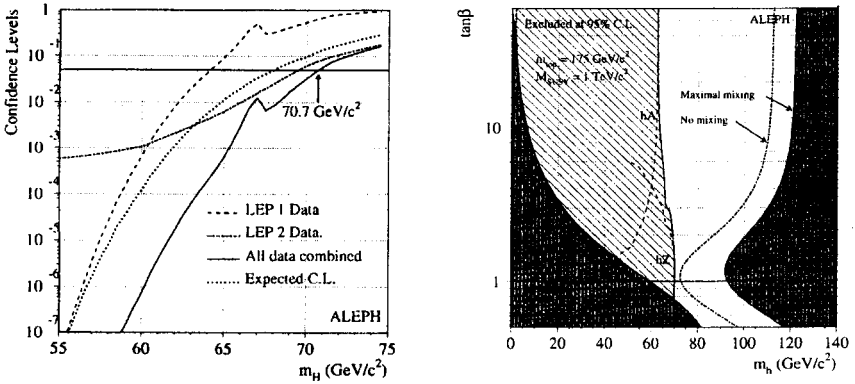

Fig. 12. Left) Preliminary SM Higgs mass confidence levels, combined for the ALEPH LEP1 and higher energy data. Right) MSSM $(m_h, \tan\beta)$ plane: the dark areas are theoretically disallowed for maximal stop mixing, the shaded area is excluded at 95% CL by the ALEPH combined search for $e^+e^- \to hZ$ and hA.

In the MSSM the 95% CL level curves for hZ and hA productions have been combined in the $(\tan\beta, m_{\mathrm{h}})$ plane, resulting in $m_h, m_A < 62.5$ GeV/c^2 for any $tan\beta > 1$, as in Fig. 12.

7. Further supersymmetry searches

Supersymmetry searches are based on topological criteria suggested by the main decays of most basic SUSY particles as charginos, neutralinos, sleptons and squarks, that may be produced at LEP2 in processes as: $e^+e^- \to \chi^+\chi^-, \chi\chi', \tilde{\ell}^+\tilde{\ell}^-, \tilde{\mathrm{t}}\bar{\tilde{\mathrm{t}}}$.

7.1. R-parity conserving SUSY

When R-parity is conserved, all events contain two neutralinos, assumed to be the Lightest Supersymmetric Particles (LSP), which carry away energy, while the visible products can contain quarks, leptons or photons. The expected topologies are therefore: four jets, two jets and one lepton, two acoplanar jets, leptons or photons.

The kinematic properties of such events differ widely, depending on the mass difference ΔM between the produced SUSY-particle and the LSP, resembling a two-photon SM event, for small ΔM, or WW decays, for a very

light LSP. Therefore a large number of selections have been developed to cope with all possible signals. Finally the number of selected events from each analysis, in the 161-172 GeV data, has been found to be consistent with the total expected known SM backgrounds, so that limits on the MSSM parameters have been derived.

From the limits on chargino ($\chi^+\chi^-$) and neutralino ($\chi\chi, \chi\chi'$) productions, a lower limit on the lightest neutralino (LSP) mass is derived

$$m_\chi > 22 \text{ GeV}/c^2 \quad \text{at } 95\% \text{ CL}$$

valid for sneutrino masses $m_{\tilde{\nu}} > 100$ GeV/c^2, $\tan\beta > 1$, and assuming gaugino mass unification. Corresponding 95% CL exclusion limits in the (μ, M_2) plane are shown in Fig. 13.

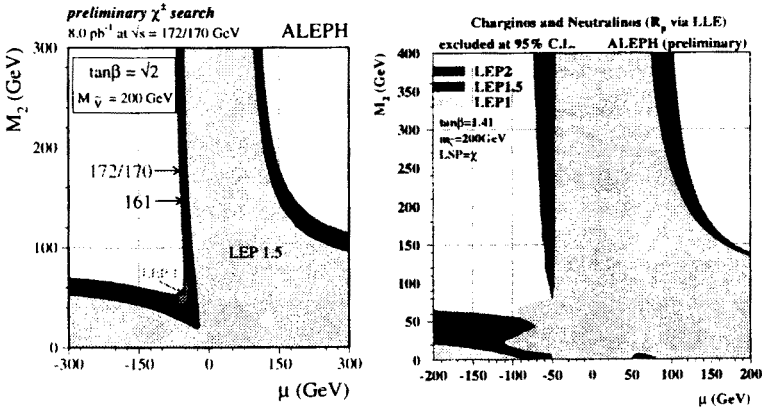

Fig. 13. Preliminary 95% CL ALEPH-excluded regions in the (μ, M_2) MSSM-plane, assuming $\tan\beta = \sqrt{2}$, $m_{\tilde{\nu}} = 200$ GeV/c^2 and LSP $\equiv \chi$, for R_p-conserving SUSY (left) and R_p-violating (right).

7.2. R-parity violating SUSY

In a SUSY model with R_p-violation, dominated by a LLE coupling term, the LSP is visible and decays as $\chi \to \ell_1^+ \ell_2^- \nu_3$, violating lepton-number. Therefore, in such scenario, final states from possible $\chi^+\chi^-, \chi\chi, \tilde{\ell}^+\tilde{\ell}^-$ and $\tilde{\nu}, \bar{\tilde{\nu}}$ productions, can consist of hadrons and leptons or only leptons, with at least four leptons and less missing energy than with previous R_p-conserving assumptions.

Again for all dedicated selections, no significant excess was found in the data with respect to the expected SM backgrounds, and limits in the MSSM have been derived with a conservative model-independent approach

and no assumption on the magnitude of the Yukawa LLE-coupling. Excluded regions in the (μ, M_2) plane are shown in Fig. 13, and are similar to the R_p conserving exclusions as such searches reach the same kind of kinematic limits.

8. Anomalous four jet events

The four jet final state has been analysed to search for hadronic decays of generic pair-produced heavy particles, following the anomalous excess observed by ALEPH at $\sqrt{s}$ =130–136 GeV [32]. The selection have therefore been repeated with the same, $\sqrt{s}$-rescaled cuts, rejecting radiative hadronic events and reconstructing four *hard* Durham-jets with large multiplicities and masses. The jets are then paired in the configuration that minimises the dijet masses difference, in the hypothesis of pair-production of equal mass particles. Final cuts are applied to reject hadronic WW decays, the only difference respect to the lower energy analysis.

As it can be seen in Fig. 14, an anomalous excess of events with respect to SM predictions is again visible in the higher energy data, though with a quite smaller measured cross-section. The whole data sample from 130 to 172 GeV shows a clear excess for a dijet mass sum of 106 GeV/c^2.

The origin of such excess is still unclear and could be due to some experimental problem arising during the data analysis. For this reason the anomalous events are currently investigated carefully by all LEP collaborations together with the features of the ALEPH reconstruction algorithms and the jet clustering.

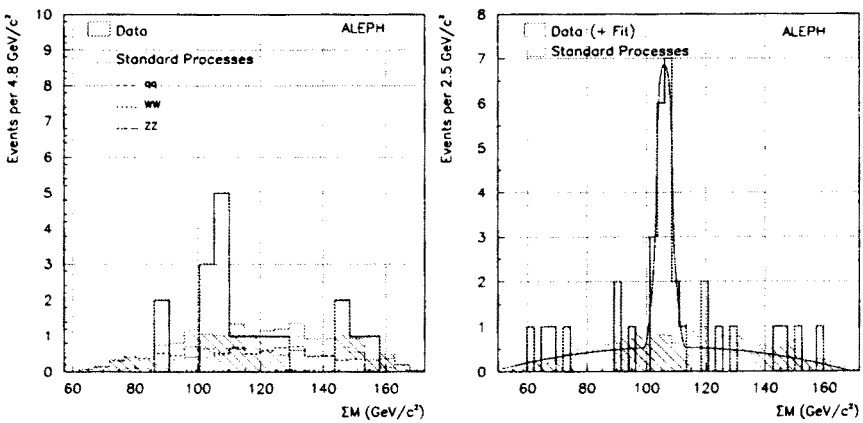

Fig. 14. Preliminary ALEPH four-jet analysis results. Mass spectrum of the dijet mass sum from the 161–172 GeV 1996 data (left), and for all data from $\sqrt{s}$ = 130 to 172 GeV (right).

9. Summary and conclusions

During the successful 1996 LEP physics runs above the nominal W-pair production threshold, the ALEPH experiment has collected about 11pb^{-1} of data at $\sqrt{s} = 161$ GeV and 11pb^{-1} at 172 GeV.

The recorded data has been analysed confirming the validity of the Standard Model both in the QCD and electroweak sectors at such previously unexplored energies and, most of all, showing the production of the first W-pair events in all decay modes. From the WW-production cross-sections and by direct reconstruction of WW decay products, two independent precision measurements of m_W, a fundamental parameter in the SM, have been obtained yielding $m_W = 80.39 \pm 0.25$ GeV/c^2. Also from the partial WW-decay cross-sections, a first direct measurement of the hadronic Branching ratio of the W has been obtained as $Br(W \to q\bar{q}') = 69.4 \pm 3.8\%$.

No evidence for the production of a Higgs sector particle has been found in the data, leading to $m_H > 70.7$ GeV/c^2 in the Standard Model, and $m_h, m_A > 62.5$ GeV/c^2 in its minimal supersymmetric extension, both at 95% Confidence Level. All further searches for possible productions of supersymmetric partners of known particles found no evidence as well in the data, so that many limits on possible SUSY scenarios have been extended.

This first bunch of LEP2 data has therefore represented an important improvement of the knowledge of the Standard Model, even though most measurements suffer from the lack of statistics. For this reason, and for a secret hope to observe a physics signal beyond the SM, ALEPH and all LEP experiments are looking forward for the next data that will be delivered in the following years, with larger integrated luminosities and higher $\sqrt{s}$ =184–200 GeV energies.

REFERENCES

[1] UA1 Collaboration, G. Arnison *et al.*, *Phys. Lett.* **B122**, 103 (1983); UA2 Collaboration, M. Banner *et al.*, *Phys. Lett.* **B122**, 476 (1983).

[2] UA1 Collaboration: G. Arnison *et al.*, *Phys. Lett.* **B134**, 469 (1984); *Europhys. Lett.* **1**, 327 (1986); C. Albajar *et al.*, *Z. Phys.* **C44**, 15 (1989); UA2 Collaboration: R. Ansari *et al.*, *Phys. Lett.* **B186**, 440 (1987); J. Alitti *et al.*, *Phys. Lett.* **B241**, 150 (1990); *Phys. Lett.* **B276**, 354 (1992); CDF Collaboration: F. Abe *et al.*, *Phys. Rev. Lett.* **65**, 2243 (1990); F. Abe *et al.*, *Phys. Rev.* **D43**, 2070 (1991); *Phys. Rev. Lett.* **75**, 11 (1995); *Phys. Rev.* **D52**, 4784 (1995).

[3] World average presented by M.Rijssenbeek at ICHEP'96, Warsaw.

[4] J. Ellis, R. Peccei eds., Physics at LEP, CERN 86-02, 1986 vol.2, p.27; A. Ballestrero *et al.*, Determination of the Mass of the W Boson, in Physics at LEP2, CERN 96-01 vol.1, p.141.

[5] Working group on LEP Energy, R. Assman *et al., Z. Phys.* **C66**, 567 (1995); LEP EG/ 96-05.

[6] Working group on LEP Energy, LEP EG/97-01.

[7] ALEPH Collaboration, D. Decamp *et al., Nucl. Istrum. Methods* **A294**, 121 (1990).

[8] ALEPH Collaboration, D. Buskulic *et al., Nucl. Istrum. Methods* **A360**, 481 (1995).

[9] G. Batignani *et al.*, 1991 IEEE Nuclear Science Symposium, Santa Fe, *IEEE Trans. Nucl. Sci.*, NS-39(4/5), 438 vol 1.

[10] G. Barber *et al., Nucl. Istrum. Methods* **A279**, 212 (1989).

[11] W.B. Atwood *et al., Nucl. Istrum. Methods* **A306**, 446 (1991).

[12] ALEPH Collaboration, D. Buskulic *et al., Phys. Lett.* **B313**, 535 (1993); *Nucl. Istrum. Methods* **A346**, 461 (1994).

[13] ALEPH Collaboration, D. Decamp *et al., Z. Phys.* **C53**, 375 (1992).

[14] S. Jadach *et al.*, `BHLUMI` 2.01, *Phys. Lett.* **B253**, 469 (1991); *Phys. Lett.* **B260**, 173 (1991); *Comput. Phys. Commun.* **70**, 305 (1992).

[15] ALEPH Collaboration, D. Decamp *et al., Z. Phys.* **C48**, 375 (1990); *Z. Phys.* **C53**, 1 (1992); D. Buskulic *et al., Z. Phys.* **C60**, 71 (1993); *Z. Phys.* **C62**, 539 (1994).

[16] ALEPH Collaboration, D. Buskulic *et al., Phys. Lett.* **B378**, 373 (1996).

[17] T. Sjöstarnd, *Comput. Phys. Commun.* **82**, 74 (1994); Lund Univ. Report LU TP 95-20 (1995).

[18] T.Sjöstarnd, *Comput. Phys. Commun.* **39**, 347 (1986); T. Sjöstarnd, M. Bengtsson, *Comput. Phys. Commun.* **43**, 367 (1987); T. Sjöstarnd, H.U. Bengtsson, *Comput. Phys. Commun.* **46**, 43 (1987).

[19] S. Jadach, B. Ward, Z. Wąs, *Comput. Phys. Commun.* **79**, 503 (1994).

[20] H. Anlauf *et al., Comput. Phys. Commun.* **79**, 466 (1994).

[21] ALEPH Collaboration, D. Buskulic *et al.*, CERN-PPE 96-186, to appear in *Phys. Rep.*

[22] ALEPH Collaboration, D. Buskulic *et al.*, CERN-PPE 96-43, submitted to *Phys. Lett.* **B**.

[23] G. Marchesini *et al., Comput. Phys. Commun.* **67**, 465 (1992).

[24] L. Lönnblad, *Comput. Phys. Commun.* **71**, 15 (1992).

[25] JADE Collaboration: W. Bartel *et al., Z. Phys.* **C33**, 23 (1986); S. Bethke *et al., Phys. Lett.* **B213**, 235 (1988).

[26] W. Stirling, Proceedings of the Durham Workshop, *J. Phys. G: Nucl. Part. Phys.* **17**, 1567 (1991); N. Brown, W. Stirling, *Phys. Lett.* **B252**, 657 (1990); S. Bethke, Z. Kunszt, D. Soper, W. Stirling, *Nucl. Phys.* **B339**, 393 (1992).

[27] M. Skrzypek, S. Jadach, W. Płaczek, Z. Wąs, *Comput. Phys. Commun.* **94**, 216 (1996).

[28] F.A. Berends, R. Pittau, R. Kleiss, *Comput. Phys. Commun.* **85**, 437 (1995).

[29] D. Bardin, D. Lehner, A. Leike, A. Olshevsky, T. Riemann, hep-ph 9603438; *Phys. Lett.* **B344**, 383 (1995); *Nucl. Phys. Proc. Suppl.* **37B**, 148 (1994); DESY 93-035.

[30] Z. Ajaltouni *et al.*, Triple Gauge Boson Couplings, in Physics at LEP2, CERN 96-01 vol.1, p.141.
[31] P. Janot, The HZHA generator, in Physics at LEP2, CERN 96-01 vol.2, p.309.
[32] ALEPH Collaboration, D. Buskulic *et al.*, *Z. Phys.* **C71**, 179 (1996).